

<https://doi.org/10.1038/s42003-024-07188-0>

Elucidating metabolic tuning of mixed purple phototrophic bacteria biofilms in photoheterotrophic conditions through microbial photo-electrosynthesis

Check for updates

Sara Díaz-Rullo Edreira¹, Ioanna A. Vasiliadou², Amanda Prado ³, Juan José Espada ¹, Ruddy Wattiez⁴, Baptiste Leroy⁴, Fernando Martínez ¹ & Daniel Puyol ¹ ✉

Reducing greenhouse gas emissions is critical for humanity nowadays, but it can be beneficial by developing engineered systems that valorize CO₂ into commodities, thus mimicking nature's wisdom. Purple phototrophic bacteria (PPB) naturally accept CO₂ into their metabolism as a primary redox sink system in photo-heterotrophy. Dedicated use of this feature for developing sustainable processes (e.g., through negative-emissions photo-bioelectrosynthesis) requires a deep knowledge of the inherent metabolic mechanisms. This work provides evidence of tuning the PPB metabolic mechanisms upon redox stressing through negative polarization (−0.4 and −0.8 V vs. Ag/AgCl) in photo-bioelectrochemical devices. A mixed PPB-culture upregulates its ability to capture CO₂ from organics oxidation through the Calvin-Benson-Bassam cycle and anaplerotic pathways, and the redox imbalance is promoted to polyhydroxyalkanoates production. The ecological relationship of PPB with mutualist bacteria stabilizes the system and opens the door for future development of photo-bioelectrochemical devices focused on CO₂ up-cycling.

Significant efforts on carbon dioxide emissions reduction push the European Union to decouple greenhouse gases (GHG) emissions from economic growth, achieving 17% of GHG emissions mitigation compared to the 45% of the overall economy increase in the last two decades¹. However, more efforts are needed to comply with the United Nations Framework Convention on Climate Change². In line with EU targets, carbon capture utilization and storage technologies are essential in contributing directly to CO₂ reduction emissions in crucial sectors (i.e., fossil-fueled power production), leading the world to a net-zero CO₂ emission path³. Based on circular economy and sustainability principles, biological technologies converting CO₂ into value-added products are being developed to produce chemicals (polymers, plastics, carbonates) and energy carriers (methane, ethane, methanol, syngas)⁴. The biological fixation of CO₂ is an attractive issue with good scale-up potential due to its low cost, self-regenerative activity, and mild reaction conditions⁵. The Calvin-Benson-Bassham (CBB) cycle is one of the critical biochemical cycles in photosynthetic organisms incorporating CO₂ into carbon metabolism. It is responsible for more than

90% of CO₂ fixation in nature, whereas the rest is through alternative autotrophic CO₂-fixing pathways, such as reductive citric acid cycle (rTCA) and reductive acetyl-CoA route⁵. Recently, photosynthetic proteobacteria known as purple phototrophic bacteria (PPB) received significant attention in environmental biotechnological systems for CO₂ fixation^{6,7}. PPB are a group of anaerobic, facultative microorganisms that absorb infrared irradiation (IR) through their photosystem (carotenoids and bacteriochlorophylls) and convert it into chemical energy⁸. These bacteria exhibit high growth rates, are not inhibited by O₂, and have a versatile metabolism that allows them to grow in variable environments via photoautotrophy, photoheterotrophy, and fermentation⁹.

The primary mechanism of CO₂ fixation by PPB under photo-heterotrophic growth is via the CBB cycle for maintaining redox homeostasis^{10,11}. Another mechanism under photoheterotrophic growth that serves as an electron sink for the cumulative reduced factors is the ATP-driven process of H₂ production under nitrogen-fixing conditions via the nitrogenase/hydrogenase enzyme complex^{12,13}. Finally, PPB can dissipate

¹Department of Chemical and Environmental Engineering, High School of Experimental Sciences and Technology, University Rey Juan Carlos, Madrid, Spain.

²Department of Environmental Engineering, Democritus University of Thrace, Xanthi, Greece. ³Department of Automation, Electric Engineering and Electronic Technology, Polytechnic University of Cartagena, Cartagena, Spain. ⁴Laboratory of Proteomics and Microbiology, Research Institute for Biosciences, University of Mons, Mons, Belgium. ✉e-mail: daniel.puyol@urjc.es

excess electrons under photoheterotrophic conditions by storing carbon in the cytoplasm, leading to polyhydroxyalkanoates (PHAs, bioplastics) generation⁷. PHAs are accumulated through the consecutive reduction of acetyl-CoA to (R)-3-Hydroxybutyryl-CoA, which is further reduced to PHA via PHA synthase (PhaC)¹⁴. PHA biosynthesis from PPB is highly affected by the oxidation state of organic carbon used as a source of electrons under photoheterotrophic conditions, where reduced organics like butyrate enhance PHA accumulation¹⁵. In contrast, oxidized organics like malate hinder PHA accumulation due to a lack of electrons¹⁶. Therefore, the number of electrons given by the carbon substrate during PPB growth significantly affects their metabolic system¹¹.

Stressing the PPB metabolic machinery through redox imbalance greatly enhances PHA production, as recently demonstrated through proteomic analysis over *Rhodospirillum rubrum*¹⁷. An exciting way to allow redox imbalance over the PPB's metabolic system is via direct electron transfer from a solid-phase conductive electrode using bioelectrochemical systems (BES). These are considered promising and environmentally friendly technologies where microorganisms are forced to a bidirectional electron transfer with electrically conductive abiotic surfaces (the electrodes) to catalyze redox reactions for power generation, electrosynthesis, or environmental sanitation¹⁸. Recycling CO₂ into organic bio-products through microbial electrochemical synthesis (MES) has been extensively studied^{19,20}. However, very few studies investigated the role of PPB's photoelectrochemical growth in the acceleration of electron sinks. Bose et al. pioneered the demonstration of the direct electron transfer from a poised graphite cathode electrode to a biofilm of iron-oxidizing *Rhodospseudomonas palustris* TIE-1 grown with CO₂ as the sole carbon source (photoautotrophy)²¹. Authors linked the electron uptake with c-type cytochromes, achieving CO₂ fixation through the RuBisCO enzyme in the CBB cycle. Rengasamy et al. correlated the electron uptake by *R. palustris* TIE-1 during photoelectroautotrophic growth to biomass production using a graphite cathode modified with an iron complex²². Guzman et al. connected the extracellular electron uptake of *R. palustris* from poised electrodes to the photosynthetic electron transport chain (pETC), while the CBB cycle using RuBisCO enzyme was the primary electron utilization pathway for CO₂ fixation²³. Li et al. examined the photoautotrophic H₂ production of *Rhodobacter sphaeroides* with CO₂ uptake in a BES using a carbon-felt cathode²⁴. Liao et al. used proteomic analysis to explore the CO₂ bioreduction behavior of *R. palustris* CGA009 under different cathodic potentials²⁵. Results showed that the electron uptake improves energy generation (through ATP) by driving electrons through NAD(P)-binding domain-containing proteins, generating NADH, and that energy enhances CO₂ fixation in the CBB cycle. Finally, Rengasamy et al. also showed that *R. palustris* TIE-1 could dissipate the excess electrons from an electrode coated with an iron-based redox mediator through the PHA accumulation²². Nevertheless, the route for cathodic electrons entering the PPB metabolism remains unknown.

All the above photo-BES studies were conducted using pure culture systems; however, exporting these achievements to a scalable system must irremediably follow the mixed-culture way²⁶. It is the only economically practical solution, especially in environmental biotechnology systems requiring long-term stability, non-sterilized conditions, and suffering from a fluctuating environment. In this sense, Vasiliadou et al. used a mixed culture of PPB that successfully utilized a graphite electrode as an electron donor for the bioelectrosynthesis of H₂¹². They reported that the redox imbalance was regulated by promoting the CO₂ fixation sink, decreasing CO₂ emissions drastically, rather than the H₂ production rate, as compared to electrode-free biological processes. Recently, Díaz-Rullo Edreira et al. examined the effect of biocathode polarization on CO₂ fixation by a mixed PPB culture under photoheterotrophic growth²⁷. Results revealed that CO₂ fixation via the CBB cycle was the main electron sink at voltages between -0.2 and -0.4 V (vs. Ag/AgCl). However, the relationship between the soluble carbon uptake and the electron consumption at voltages between -0.6 and -0.8 V (vs. Ag/AgCl) indicated that other electron sinks were involved. Even though the abovementioned studies showed for the first time the enhanced bioelectrochemical CO₂ fixation under photoheterotrophic

conditions, the entire set of metabolic paths regulated under redox imbalance by the microbial consortia of a mixed PPB biocathode has not been investigated yet, which is a critical gap for enabling the scalability of photo-BES systems.

Based on the above, this work aims to elucidate the metabolic pathways involved in the redox balancing process of a PPB mixed biofilm grown under photobioelectrochemical and heterotrophic conditions. For this purpose, we focus on three main objectives: (i) the analysis of the structure of the microbial consortia of mixed PPB biofilm; (ii) the effect of applied potentials (-0.4, -0.8 V vs. Ag/AgCl) on the activation of different metabolic processes; and (iii) the study of the central metabolic routes affected by the electrons from the cathode, such as extracellular electron transfer (EET), CBB and anaplerotic routes (CO₂ fixation), TCA, Glyoxylate bypass (organic carbon oxidation), and PHA accumulation. These will provide a deeper insight into photo-bioelectrochemical processes developed onto biocathode under different potentials applied with biotechnological (technology development), environmental (carbon dioxide reduction), and socioeconomic (product development) interests.

Results

Structure of the microbial consortia of mixed PPB biofilm

The two photoelectrochemical experiments were conducted after the start-up period of PPB acclimation and biofilm formation onto the cathode electrode (see Supplementary Fig. S1). First, the absorbance peaks at 805 and 865 nm via VIS-NIR spectra analysis demonstrated the development of a biofilm rich in PPB (see Supplementary Fig. S2), as these wavelengths are typically used by the light-harvesting system of PPB that contains bacteriochlorophyll *a* (*BChla*). This analysis was performed daily throughout the operation of the system.

Figure 1 shows the abundance of the different genera in the mixed PPB biofilm in each experiment. The abundance of PPB under light conditions was 33–50%, where two genera (*Rhodospseudomonas* and *Rhodobacter*) covered almost the full PPB range, being more abundant in the -0.4 V experiment than in the -0.8 V one. These data agree with the screenings of the absorbance spectra measured during the experiments (805 and 865 nm) corresponding to *BChla* (Supplementary Fig. S3). Figure 1 also exhibits the presence of other electroactive genera, such as *Shewanella*, *Raoultella*, *Pseudomonas*, or *Desulfovibrio*, but their abundance was not significant compared to PPB genera. Thus, their contribution to the photo-BES performance was not relevant. However, the non-electroactive genus *Wolinella* presented an important abundance (19–47% under light conditions and increased to 63% in the dark open circuit -DOC- control experiment) in the mixed biofilm, which suggests some ecological relation between this genus and PPB genera that will be further discussed.

Effect of applied potentials on the activation of different metabolic processes

Chronoamperometry allowed the evaluation of the capacity of the biofilm to interact with the electrode during BES operation. Figure 2a shows the chronoamperograms of the two photo-bioelectrochemical experiments and the control (open circuit) experiment obtained by recording the electrochemical interaction between the PPB mixed biofilm and the working electrode during the first four days of the second week of operation. Chronoamperograms at -0.4 V and -0.8 V (vs. Ag/AgCl) show a significant cathodic behavior, resulting in a net electron consumption, with the -0.8 V experiment significantly more active than the -0.4 V one. The jumps in the electricity current are due to the cyclic voltammeteries performed on days 0, 2, and 4. Figure 2a also shows the chronoamperogram of the abiotic control (-0.8 V vs. Ag/AgCl), which did not exhibit any significant redox interaction. These data mean the cathodic behavior from photobioelectrochemical experiments is due to the presence of the biofilm on the cathode and, consequently, because of an extracellular electron transfer (EET) route intervention. To assess the robustness of the experimental design concerning the assumption of achieving a steady state after one week of operation at a specific voltage, an in-depth chronoamperometry analysis

Fig. 1 | Abundance of different genera present in the PPB mixed biofilm for each experiment as determined by 16S rRNA gene amplicon sequencing with Illumina MiSeq: initial and final. The sample -0.4 V initial showed not representative data (not shown).

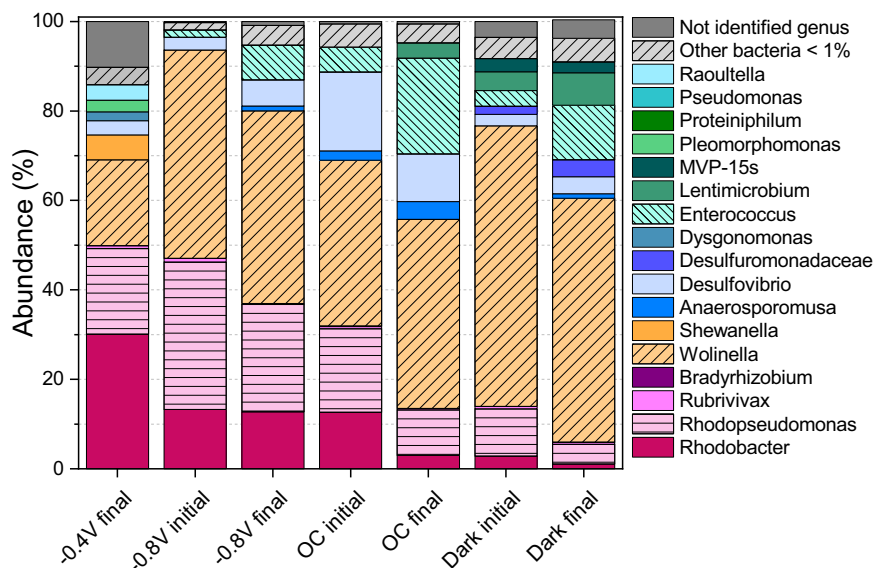
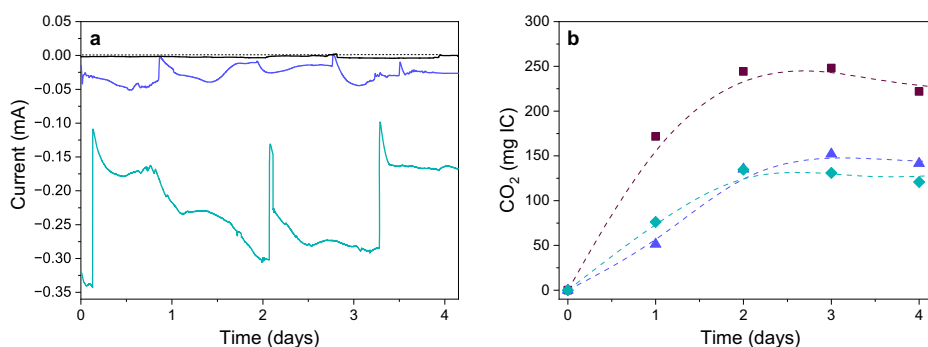


Fig. 2 | Bioelectrochemical and carbon fixation response of the experiments during the second week. Chronoamperograms of each experiment carried out: Electrochemical control (black line), -0.4 V (dark blue line) and -0.8 V (light blue line) (a). CO_2 time-course: Open Circuit control (purple squares), -0.4 V (dark blue triangles) and -0.8 V (light blue diamonds) (b).



spanning the entire experimental duration reveals the system's stability during the second and third weeks. Detailed insights can be found in the Supporting Information (Supplementary Fig. S3).

The analysis of the CO_2 fixation was performed by measuring the CO_2 fate in the system. In this sense, malic acid is a perfect substrate for this analysis since it is more oxidized than the biomass, and its uptake generates CO_2 . Thus, the evolution of CO_2 in the system can provide evidence for CO_2 fixation. Figure 2b exhibits the time course of CO_2 production (as inorganic carbon, IC). pH values added in Supporting Information, Supplementary Table S1) in photo-bioelectrochemical and OC control experiments. The CO_2 production derived from the oxidation of malic acid is significantly lowered in bioelectrochemical conditions at both potentials. This entails an activation of the CO_2 fixation pathways, which result from the excess electrons supplied to the BES.

Hydrogen production in the BES system was not observed. The presence of ammonium as the nitrogen source explains this, as it is a strong inhibitor of nitrogenase. Also, the abiotic control experiment at -0.8 V (vs. Ag/AgCl) showed no electrochemical activity, as seen in Fig. 2a. Nevertheless, as previously documented, hydrogen evolution in biocathodes cannot be dismissed at potentials ranging from -0.7 to -0.9 V. Notably, studies³⁸ have demonstrated H_2 production rates in this voltage range, ranging from 0.31 to $2.4 \text{ m}^3/\text{m}^3\cdot\text{d}$. Hence, the observed rise in current density during the -0.8 V experiment might be attributed, at least in part, to hydrogen production in the biocathode.

The effect of the bioelectrochemical conditions over the TCA cycle was studied by analyzing the evolution of short-chain carboxylic acids (SCCAs) in terms of chemical oxygen demand (COD). Figure 3 presents the time

course of COD and SCCAs during the second week of operation for the two experimental cycles (-0.4 and -0.8 V vs. Ag/AgCl) and the OC experiment performed. The appearance of fumaric acid as the only SCCA from malic acid catabolism strongly indicates that the central catabolism follows the reductive TCA cycle. In all cases, the final COD did not match with SCCA, likely due to the release of non-HPLC-measurable allogenetic organic matter by the mixed consortia³⁹. In any case, the COD uptake rate in the OC was 215 mg COD/d , whereas the values rose to 393 and 383 mg COD/d at -0.4 and -0.8 V, respectively. In addition, Fig. 3a shows an excess of undefined COD in the OC experiment that limited the COD consumption rate. In contrast, the COD in the BES was close enough to the sum of the detected SCCAs (malic and fumaric acids). Thus, the biological electron's uptake from the cathode enhanced the heterotrophic uptake processes.

The analysis of the anabolic reactions was performed by direct observation of the microbial growth. Figure 4 illustrates the initial and final biomass concentrations at the photoelectrochemical and OC experiments. The available electrode's surface for biofilm development was limited in these experiments, so the biomass mainly grows in a planktonic form where they do not have space limitations. Nevertheless, the average suspended culture growth exhibited under photoelectrochemical conditions was significantly higher (at 95% confidence level) than the suspended culture growth in the OC control: 1939 ± 75 , 2319 ± 29 , and $2942 \pm 202 \text{ mg COD/L}$ for OC, -0.4 and -0.8 V, respectively. The biomass growth was, therefore, significantly more efficient in bioelectrochemical conditions.

Accumulative processes were studied by analyzing the production of PHA. Figure 5 exhibits the amount of PHA (expressed as % in mass units) accumulated during photo-bioelectrochemical experiments compared to

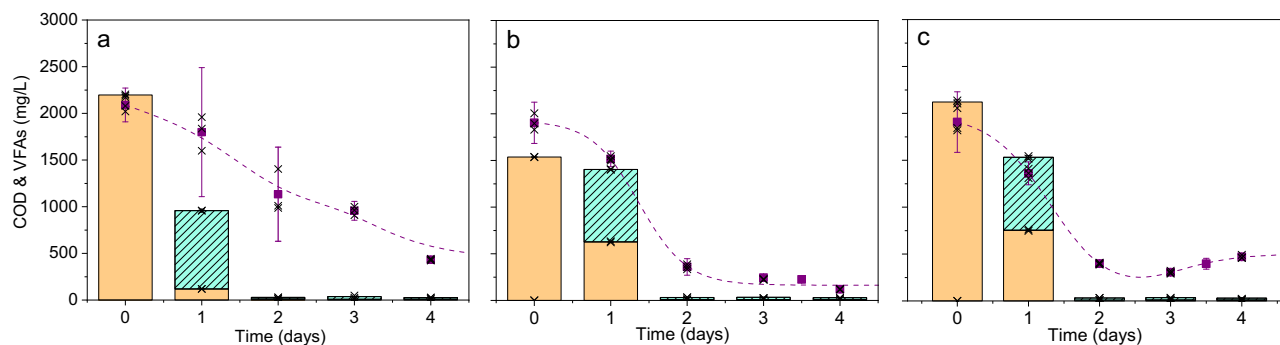


Fig. 3 | Effect of applied voltage on the growth and carbon assimilation during the second week of the bioelectrochemical experiments. Time course of the COD (purple squares) and SCCA (columns), where orange represents malic acid, and light striped blue is fumaric acid: Open Circuit control (a), -0.4 V (b) and -0.8 V (c). Error bars are 95% confidence intervals from triplicate measurements. Individual data points are included.

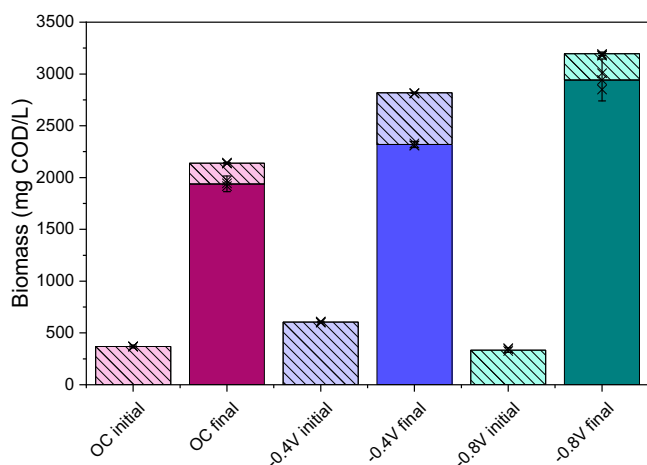


Fig. 4 | Biomass in mg COD/L analyzed from the liquid medium and from biofilm (stripped area) for each experiment carried out: open circuit (pink), -0.4 V (blue) and -0.8 V (green). Error bars are confidence intervals (at 95%) from triplicate measurements.

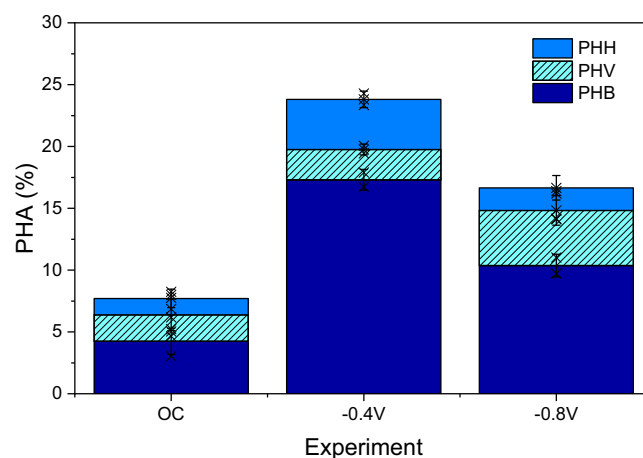


Fig. 5 | Percentage of PHAs accumulated by the PPB mixed biofilm under electrochemical conditions and in the OC control: polyhydroxybutyrate (PHB, dark blue), polyhydroxyvalerate (PHV, striped light blue), and polyhydroxyhexanoate (PHH, light blue). Error bars are 95% confidence intervals from triplicate measurements.

the OC control. The amount of each PHA bioaccumulated, expressed as average mgPHA/L \pm 95% confidence intervals from triplicate measurements, was 58 ± 3 and 18 ± 2 mg poly-3-hydroxybutyrate (PHB)/L; 8 ± 1 and 8 ± 2 mg polyhydroxyvalerate (PHV)/L; 14 ± 2 and 3 ± 2 mg polyhydroxyhexanoate (PHH)/L, for -0.4 and -0.8 V (vs. Ag/AgCl), respectively. Results showed that the artificial addition of reduced cofactors to PPB's metabolism through the conductive electrode enhanced the accumulation of PHA despite using malic acid as a carbon source. Besides, the voltage applied to the system had an evident influence on PHA accumulation in PPB from the biofilm, showing a higher amount of PHA (at 95% confidence level) at -0.4 V (23.8% of total PHA). However, at -0.8 V , this percentage of accumulated PHA decreased, which could be attributed to less biofilm attached to the biocathode (Fig. 3) since the direct electron transfer from the cathode to the suspended PPB is limited. It may also be related to a lower presence of PHA-accumulating microorganisms in the consortium, as will be commented on later. The bioelectrochemical mediation of the enhancement of PHA accumulation was significantly evident at a 95% level for both cathodic potentials compared to the OC.

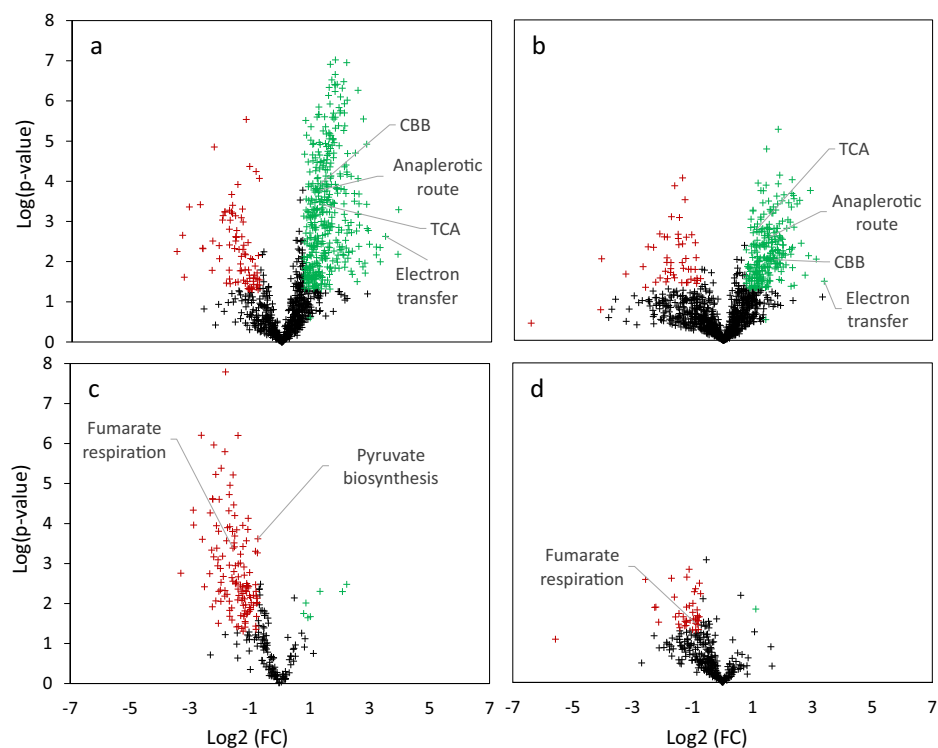
Elucidating the main metabolic routes affected by external electrons

Metaproteomics drove the analysis of the effect of bioelectrochemical conditions on the metabolism of the mixed PPB cultures. Figure 6 shows the volcano plots obtained from metaproteomic data obtained for the proteins

of the different genera of PPB (Fig. 6a, b) and the proteins of *Wolinella* (Fig. 6c, d) at the reactor's level (e.g., accounting for the total amount of proteins detected in the reactor). This figure exhibits an essential amount of statistically relevant data to analyze metabolic pathways affected by the tested photoelectrochemical conditions. On the one hand, the photoelectrochemical conditions provoked an increase of abundance in the two main PPB genera presented in the biofilm, consequently increasing, at the reactor's level, most of the proteins from PPB, like enzymes related to the CBB and TCA cycles, the anaerobic CO_2 fixation pathways and the electron transfer proteins. These data reveal that the photoelectrochemical conditions presented a favorable environment for PPB development and, consequently, for incrementing PPB's key enzymes. Table 1 shows the regulation of main proteins from the most relevant metabolic pathways.

On the other hand, volcano plots of *Wolinella* show the decrease of this bacteria under photoelectrochemical conditions compared to the OC experiment and, therefore, the reduction of almost all enzymes analyzed for this genus. Key examples are the enzymes related to fumarate respiration or pyruvate synthesis. The maintained abundance of *Wolinella* in the consortium suggests that this genus found different ways to develop this part of its metabolism at the reactor's level, like a commensalism relation between this genus and PPB genera, which will be further analyzed in the Discussion section.

Fig. 6 | Raw metaproteomic data of the experiments during the third week at the reactor's level. Volcano plots of metaproteomic data from PPB genera: *−0.4 V/OC* (a), *−0.8 V/OC* (b), and *Wolfinella* sp.: *−0.4 V/OC* (c), *−0.8 V/OC* (d). Black points indicate non-representative (p -value > 0.05) fold change with respect to the open circuit, whereas red and green points indicate representative (p -value < 0.05) negative and positive fold changes with respect to the open circuit, respectively. Proteins related to the main metabolic processes of interest are indicated within the charts.



Discussion

The first metabolic pathway studied was the extracellular electron transfer (EET), mediated by some proteins such as porin, c-type, b-type, and ubiquinol cytochromes for the *Rhodospseudomonas* genus. Hence, regulating these proteins is of enormous interest in this research.

The chronoamperograms from each experiment (Fig. 2a) demonstrate that the mixed biofilm interacted with the electrode. Also, the substantial amount of PPB genera in the biofilm in photoelectrochemical experiments (Fig. 1) corroborates that the electrochemical conditions promoted the growth of these genera over the graphite bar. Additionally, the bioelectrochemical biomass growth, in contrast to OC control (Fig. 4), suggests that the excess electrons supported the biomass growth, considerably increasing the final biomass measured. Another evidence is the formal potential of photo-bioelectrochemical experiments, taken from the cyclic voltammetry (CV) of each experiment on day two according to the apparent midpoint potential ($E_{1/2}$)³⁰ as shown in Supporting Information (Supplementary Fig. S4), when the substrate was consumed (non-turnover conditions) (Supplementary Fig. S5). These potentials (expressed as E (V vs. SHE)) were 0.12 V for the -0.4 V (vs. Ag/AgCl) experiment and 0.2 V for the -0.8 V (vs. Ag/AgCl) one, which are inside the range of redox potential of c-type cytochromes: -0.4 to 0.2 V (vs. SHE)^{31–35}. These measurements are similar to the midpoint redox potential reported for *Rhodospseudomonas palustris* pure cultures²¹. The presence of the identified redox pair implies the existence of components with redox activity that may play a role in the uptake of extracellular electrons. Consequently, the electrochemical analysis of the consortium strongly indicates the potential for direct extracellular electron transfer in which the redox site could be involved. However, different c-type cytochromes are involved in the electron transfer process with very similar redox potentials, making it difficult to determine the exact potential of each cytochrome involved using only CV data³⁰. The EET mechanism for *Rhodospseudomonas* involves c-type cytochromes, b-type and ubiquinol cytochromes, and porin proteins. Despite the trends observed in the electrochemical response, it is difficult to establish a direct connection between the midpoint potentials and CV profiles with the microbial community's specific structure and function. The electrochemical response can be attributed to different species working with mixed cultures. To

comprehend the underlying dynamics, it is necessary to perform direct biological analyses using culture-independent methods, such as metagenomics and marker gene sequencing. Metaproteomic data showed an increase at the reactor's level of these proteins involved in EET found in *Rhodospseudomonas* for the photo-bioelectrochemical experiments (Table 1). Figure 7 shows the regulation of the main proteins from the *Rhodospseudomonas* sp. genus, as determined at the taxon's level, e.g., normalizing the data for the increase in the abundance of this genus in the consortium. In the case of *Rhodobacter* sp., the whole mechanism is not fully described in the literature. Still, the results show that the EET electrons' main door differs between *Rhodospseudomonas* and *Rhodobacter*, where the former upregulated the periplasmic cytochrome c (CitcP) (Fig. 7, with the description of acronyms found in Supplementary Tables S2 and S3 in Supplementary Information), and the latter seems to use the periplasmic c-556 cytochrome (Citic556), which are upregulated in both cases (CiticP: FC $-0.4/OC$: 2.69 and FC $-0.8/OC$: 3.09. Citc556 (A0A0Q0QW64): FC $-0.4/OC$: 7.26 and FC $-0.8/OC$: 10.50). Also, *Rhodospseudomonas* upregulated the link between the c cytochromes and the ETC through a periplasmic high-potential iron-sulfur protein (the 2Fe-2S-EP ferredoxin). However, this link was not found in *Rhodobacter*. In addition, the bc1 cytochrome of the electron transport chain (ETC) of *Rhodospseudomonas* is partially upregulated (as shown in the upregulation of some of their subunits, see Fig. 7). Nevertheless, remarkably, both genera strongly upregulated the synthesis of the ETC-associated ATPase (Table 2), which means that the cathodic electron flux mainly drives energy production. These shreds of evidence confirm that the PPB actively energizes their metabolism using cathode electrons.

Several authors studied the mechanism involved in electron transfer between the electrode and electroactive PPB, such as *Rhodospseudomonas palustris* TIE-1. These studies reveal that *R. palustris* TIE-1 encodes three protein types to mediate the external electron transfer: multiheme cytochrome c, an outer membrane porin, and a periplasmic high-potential iron-sulfur protein^{23,36–38}. Furthermore, Bose et al. linked the upregulation of genes responsible for c-type cytochrome encoding with RuBisCO protein for a pure strain of *Rhodospseudomonas palustris* TIE-1²¹. Nevertheless, the regulation of EET-mediated proteins has never been reported for mixed

Table 1 | Metaproteomic data obtained from PPB consortium at reactor’s level: proteins involved in Anaplerotic CO₂ fixation, CBB cycle, PHA synthesis, TCA cycle, GB, and EET pathways

	Accession number	Identified peptides		FC	p value	FC	p value ^a	Description
		-0.8 V/OC	-0.4 V/OC					
Anaplerotic CO ₂ fixation	A0A318TJ74	11	10	2.89	2.68E-03	2.38	1.68E-04	Phosphoenolpyruvate carboxykinase (ATP)
	A0A318TNP4	1	-	2.34	8.68E-03	-	-	Pyruvate dehydrogenase E1 component subunit beta
	A0A318TQ69	8	5	1.89	9.43E-04	1.98	1.19E-03	Pyruvate, orthophosphate dikinase
	A0A7H0XTV9	1	-	2.10	4.85E-02	-	-	Pyruvate carboxylase
	B9KNI0	-	1	-	-	2.10	4.61E-02	
	A0A318TI59	-	10	-	-	2.26	3.36E-05	Pyruvate-ferredoxin/flavodoxin oxidoreductase
	A0A318TM06	2	2	3.20	8.95E-03	2.75	4.35E-06	Enolase
	A0A3G6WLM5	7	-	0.79	3.69E-02	-	-	
	Q07ND9	1	1	3.68	6.69E-03	2.90	1.31E-04	
CBB Cycle	A0A318TE67	4	4	3.56	1.51E-02	2.21	4.46E-05	Phosphoglycerate kinase
	A0A318TVC6	7	6	3.24	9.69E-03	2.45	1.15E-04	Ribulose biphosphate carboxylase
	Q07N62	1	-	4.07	2.31E-04			Fructose-1,6-bisphosphate aldolase
	Q3IX56	-	1	-	-	0.38	1.13E-02	
	E6VEW1	-	1	-	-	0.39	1.67E-02	
	Q3J0V6	1	1	2.61	1.95E-03	1.89	2.41E-02	Fructose-1,6-bisphosphatase
	A0A318TV31	-	2	-	-	2.82	2.93E-04	
	Q3J3I7	-	3	-	-	3.92	1.51E-04	Fructose-bisphosphate aldolase
PHA synthesis	A0A318T9K1	3	2	2.06	2.86E-02	2.59	5.80E-04	3-oxoacyl-[acyl-carrier-protein] synthase I
	A0A318TML2	1	1	2.61	2.76E-03	1.74	2.51E-02	3-oxoacyl-[acyl-carrier-protein] synthase II
	A0A318TA66	2	3	3.37	5.59E-04	2.98	2.03E-05	3-oxoacyl-[acyl-carrier-protein] reductase /acetoacetyl-CoA reductase
	A0A318T932	-	1	-	-	4.97	7.49E-05	3-oxoacyl-[acyl-carrier protein] reductase
	A0A318T8N2	4	2	3.94	1.06E-03	6.60	2.80E-06	Acetyl-CoA acetyltransferase
	B9KLT9	-	1	-	-	4.64	1.26E-03	
	A0A7H0XVR5	1	1	0.65	4.03E-02	6.51	1.34E-02	Acetyl-CoA C-acetyltransferase
	A0A318TQH8	1	-	4.93	9.72E-05	1.86	4.08E-02	Acyl-CoA dehydrogenase
	A0A1D9MAQ9	1	-	2.82	8.76E-03	-	-	Enoyl-[acyl-carrier-protein] reductase [NADH]
	A0A318TLU6	1	-	2.81	3.16E-02	2.09	1.82E-02	Enoyl-CoA hydratase
	A0A318U0E2	-	1	-	-	0.46	4.66E-02	
	Q07QY2	-	1	-	-	2.24	3.58E-03	
	A0A7H0Y0T8	1	-	0.31	2.31E-02			Malonyl CoA-acyl carrier protein transacylase
	A0A318TFD2	3	3	4.20	7.42E-03	4.19	3.62E-04	Phasin
A0A318TJM4	-	9			1.86	2.70E-02		
A0A318TI86	14	10	2.13	1.94E-02	1.77	7.06E-06	Short chain enoyl-CoA hydratase /3-hydroxyacyl-CoA dehydrogenase	
TCA & GB	A0A318TI19	3	2	2.73	9.02E-03	2.14	4.94E-04	2-oxoglutarate ferredoxin oxidoreductase alpha subunit ^b
	A0A0Q0WES2		2	4.55	3.67E-04	1.95	7.21E-04	Citrate synthase ^c
	A0A318TKR2	4	3	2.40	1.73E-03	1.55	3.18E-03	
	A0A318TLX9	5	4	2.17	1.69E-03	-	-	
	B9KNB0	-	1	-	-	7.40	1.68E-03	Dihydrolipoyllysine-residue succinyltransferase component of 2-oxoglutarate dehydrogenase complex
	A0A318TB01	12	-	2.63	1.87E-02	-	-	Isocitrase
	Q218P8	1	1	3.60	3.27E-03	3.25	3.29E-04	Isocitrate dehydrogenase [NADP]
	A0A519G0W9	1	-	2.56	3.64E-03	-	-	Malate dehydrogenase
A0A318TJR8	6	-	4.96	1.54E-02	2.55	3.82E-04		

Table 1 (continued) | Metaproteomic data obtained from PPB consortium at reactor's level: proteins involved in Anaplerotic CO₂ fixation, CBB cycle, PHA synthesis, TCA cycle, GB, and EET pathways

Accession number	Identified peptides		FC		p value		Description	
	−0.8 V/OC	−0.4 V/OC	−0.8 V/OC	−0.4 V/OC	−0.8 V/OC	−0.4 V/OC		
A0A4V5PP73	–	2	–	–	3.25	9.47E-03		
A0A3G6W7R8	–	1	–	–	2.74	8.21E-03		
A0A1G7PCR9	–	1	–	–	0.30	1.56E-03	Malate synthase	
A0A318TAB1	7	–	0.59	2.89E-02	–	–	Malate synthase G	
A0A318TNB8	9	7	2.17	2.18E-02	2.73	5.05E-05	Methylmalonate-semialdehyde dehydrogenase [acylating]	
A0A318T8H9	5	4	1.99	4.00E-03	2.08	1.15E-05	Succinate dehydrogenase flavoprotein subunit	
A0A318TC46	3	3	1.93	4.30E-02	2.79	1.17E-04	Succinate--CoA ligase [ADP-forming] subunit alpha	
Q07UX7	1	1	2.73	9.02E-03	2.28	1.55E-04		
D5APB4	–	1	–	–	4.97	1.71E-02		
A0A330HC69	–	2	–	–	3.94	5.03E-03		
A0A318TBR7	6	5	3.23	2.07E-03	2.25	2.51E-06	Succinate--CoA ligase [ADP-forming] subunit beta	
A0A323UD73	1	–	2.92	8.71E-03	–	–		
A0A3G6WQY2	–	4	–	–	2.58	4.58E-04		
EET	A0A318TD31	6	6	4.46	9.76E-04	4.29	4.17E-06	Cytochrome c
	A0A330H6E2	2	–	0.41	3.08E-04	–	–	
	A0A330H898	–	2	–	–	1.65	2.47E-02	
	A0A318TR75	2	2	1.64	2.31E-02	2.27	2.30E-03	Ubiquinol-cytochrome c reductase iron-sulfur subunit (Rieske protein)
	A0A330HBE3	–	2	–	–	2.61	6.11E-03	
	A0A318TN21	–	3	–	–	1.42	2.97E-03	
	A0A7H0XUS3	4	3	1.29	2.78E-02	3.14	1.20E-04	Cytochrome c1
	A0A330HLV6	–	1	–	–	2.03	3.99E-02	
	A0A0Q0QW64	1	1	10.38	3.35E-02	10.99	2.35E-03	Cytochrome c556
	A0A318TEE2	1	1	3.07	1.06E-02	2.66	1.26E-03	Ferredoxin 2Fe-2S
	A0A318TNY1	2	2	4.79	4.47E-02	3.74	1.45E-02	Porin
	A0A7H0XXE9	–	6	–	–	2.48	9.99E-04	
	A0A318TIA3	–	2	–	–	3.01	2.13E-04	Cytochrome b
	A0A318U0K5	–	1	–	–	8.90	4.33E-03	NADH-quinone oxidoreductase

^aThe p value of every data on the table is <0.05

^bReverse TCA

^cTCA and Reverse TCA

cultures of PPB. Moreover, Bose et al. did not observe a significant difference in cell density with a pure strain under their electrochemical conditions (−0.1 V vs. Ag/AgCl)²¹. On the contrary, the data showed an increased culture density at lower voltages with a mixed culture of PPB (Fig. 4). This fact means that part of the electrons assimilated by bacteria is actively used to create new cells.

In conclusion, the superior growth of PPB, mainly *Rhodospseudomonas* sp., under photoelectrochemical conditions is possible thanks to their EET ability via c-type cytochrome for both genera and via porin, b-type, c-type, and ubiquinol cytochromes. In both cases, ATP production is mainly driven by generating a proton motive force between the periplasm and the cytoplasm, with the electrons coming from the direct EET via cytochromes. c. However, other potential ways described in the literature for EET, such as pilli¹⁸, have not been found in the metaproteomic data and should not be discarded. A deeper insight into the electric link between cytochromes c and solid phases is encouraged, which is out of the scope of this work.

Other metabolic pathways studied are the CO₂ fixation routes, such as CBB and anaplerotic pathways, because they are reported in the literature as electron sinks under photoelectrochemical conditions by pure strains of some PPB^{23,39,40}. As reported in Fig. 2b, the accumulated concentration of CO₂ during the electrochemical experiments decreases compared to the OC

experiment, which implies the upregulation of the CO₂ fixation process. The theoretical CO₂ produced via malic acid degradation was calculated to demonstrate the bioelectrochemical fixation of this gas in our experiments as measured from inorganic carbon (IC) uptake⁴¹. Under electrochemical conditions, the average amount of CO₂ fixed was 43.19 ± 0.06% of the total CO₂ theoretically produced from malic acid degradation, compared to 4.61% of this CO₂ being fixated in the OC experiment. In addition, Table 1 shows an increase of RuBisCO protein in photo-bioelectrochemical experiments, which is responsible for fixing CO₂ in the CBB cycle^{21,42,43}. This enzyme's fold change (FC) values at the reactor's level are 2.45 and 3.24 for −0.4 V/OC and −0.8 V/OC, respectively, which exhibit a clear increment in the abundance of this protein under lower voltages in the reactor, probably linked to the development of PPB in the consortium. However, CO₂ fixation is also happening in an anaplerotic way. These pathways are governed by pyruvate carboxylase (PC) and phosphoenolpyruvate (PEP) carboxykinase proteins^{44–47}. PEP carboxykinase increased at the reactor's level with a similar fold change for every experiment: 2.38 and 2.89 for −0.4 V/OC and −0.8 V/OC, respectively. Pyruvate carboxylase also rose under both voltages tested at the reactor's level (FC: 2.10 for both −0.4 V/OC and −0.8 V/OC) (Table 1). To provide more evidence, Fig. 7a and Fig. 7c exhibit the upregulation of RuBisCO from the *Rhodospseudomonas*

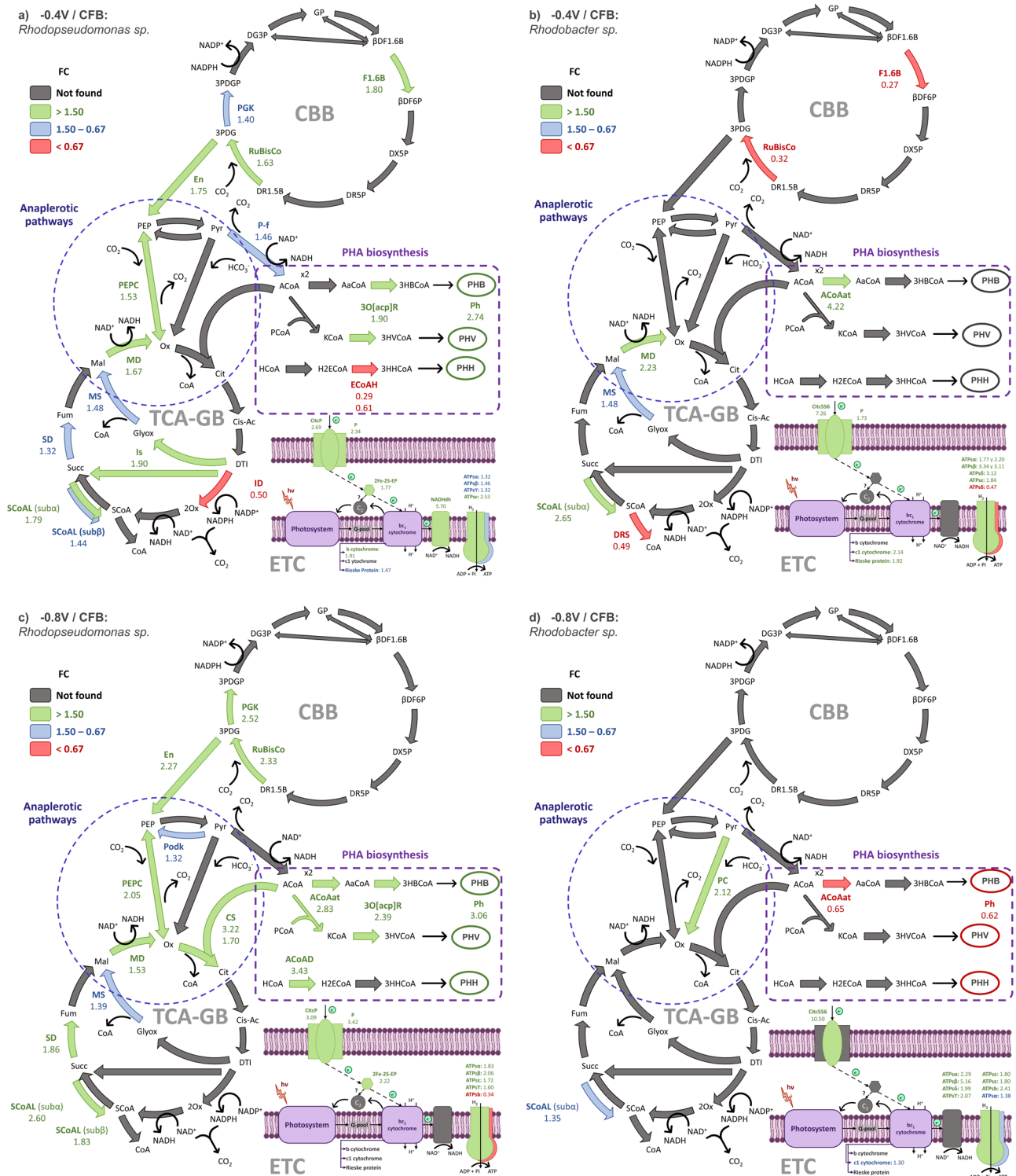


Fig. 7 | Metaproteomic regulation of PPB genera under electrochemical conditions, at taxon's level. -0.4 V/OC: *Rhodospseudomonas* sp. (a), -0.4 V/OC: *Rhodobacter* sp. (b), -0.8 V/OC: *Rhodospseudomonas* sp. (c) and -0.8 V/OC: *Rhodobacter* sp. (d) The ρ value of every data on the figure is < 0.1 . Code for the

enzymes' acronyms can be found in Supplementary Information (Supplementary Tables S2 and S3). FC fold change, CBB Calvin-Benson-Bassham cycle, TCA-GB tricarboxylic acid and glyoxylate bypass cycles, ETC electron transport chain.

genus, indicating that this species (and not *Rhodobacter*) benefitted from the electrochemical conditions that enabled CO_2 fixation as one of the central electron sinks used to dissipate the excess of electrons, even under heterotrophic conditions.

Some authors reported that the fixation of CO_2 is the primary electron sink used for PPB pure cultures to dissipate the excess of electrons under

electrochemical conditions^{23,39,40}. Still, BES based in PPB mixed cultures have not been deeply studied yet. This work shows evidence of CO_2 fixation under heterotrophic conditions when most of the literature related to CO_2 fixation works under autotrophic conditions²³.

The corroborated hypothesis describes that the CO_2 refixation process under heterotrophic conditions is due to the excess of electrons supplied to

Table 2 | Metaproteomic data obtained from *Rhodobacter* sp. at genera's level: ATP synthase protein related to EET mechanism

Accession number	Identified peptides		FC	ρ value	FC	ρ value	Description
	-0.8 V/OC	-0.4 V/OC					
A0A7H0XV71	1	2	1.80	1.38 E-02	1.84	9.37 E-03	ATP synthase epsilon chain
A0A0Q0QMK5	3		2.07	5.79 E-02	–	–	ATP synthase gamma chain
A0A0Q0QUZ8	1	1	5.16	3.74 E-02	3.34	3.19 E-02	ATP synthase subunit beta
A0A7H0XV75	2	1	1.99	5.51 E-02	3.12	3.68 E-03	ATP synthase subunit delta
A0A330HGA9	2	2	1.38	7.16 E-02	1.77	1.32 E-02	ATP synthase subunit alpha
A0A318TYK3	3	2	2.29	9.91 E-02	2.20	4.71 E-02	ATP synthase subunit alpha
A0A330HBV3	1	–	2.41	3.39 E-02	–	–	ATP synthase subunit b
A0A330HJF7	–	4	–	–	3.11	6.88 E-05	ATP synthase subunit beta
A0A330HH37	–	1	–	–	0.47	2.68 E-02	ATP synthase subunit delta

Table 3 | Metaproteomic data of fumarate respiration, and Pyruvate and phosphoenolpyruvate from *Wolinella* genus, at reactor's level

	Accession number	Identified peptides		FC	ρ value	FC	ρ value	Description
		-0.8 V/OC	-0.4 V/OC					
Pyruvate biosynthesis	Q7M7R5	–	1	–	–	0.52	9.53E-03	Pyruvate synthase alpha subunit
	Q7M9L6	–	3	–	–	0.60	2.40E-04	Phosphoenolpyruvate synthase
	Q7MAL2	–	7	–	–	0.48	7.41E-05	Malic enzyme
Fumarate respiration	P17413	2	1	0.54	3.33E-02	0.26	8.81E-03	Fumarate reductase cytochrome b subunit
	P17412	–	11	–	–	0.43	3.75E-04	Fumarate reductase flavoprotein subunit
	P17596	–	8	–	–	0.34	4.11E-04	Fumarate reductase iron-sulfur subunit

the biofilm, which provokes a redox imbalance in PPB. Hence, PPB uses some metabolic pathways as an electron sink to recover redox homeostasis^{10,11}. This imbalance is due to the excess NADH produced in phototrophic EET, consumed via the CBB cycle in the case of *Rhodospseudomonas*. In this way, the photosynthetic EET, enhanced by the excess of electrons supplied by the cathode, is indirectly linked with CO₂ fixation through the CBB cycle as an electron sink^{23,40}.

The influence of the excess of electrons on the TCA cycle was also studied, revealing this cyclic route is linked to the presence of *Wolinella* as an opportunistic microorganism. The metaproteomic data analyzed at the reactor's level demonstrate the increase of some enzymes from TCA, Glyoxylate bypass, and rTCA from the PPB (Table 1). These are the main pathways used by PPB to degrade COD. Their increase is linked to pyruvate and phosphoenolpyruvate synthesis by PPB genera through pyruvate carboxylase (PC) and phosphoenolpyruvate carboxykinase (PEPC), as it was commented before. The analysis of the proteomic data at the taxon's level, shown in Fig. 7, reveals the upregulation of some enzymes related to the TCA cycle in *Rhodospseudomonas* species (Fig. 7a, c). *Rhodobacter* did not exhibit a significant number of upregulated proteins (Fig. 7b, d) compared to *Rhodospseudomonas*. These observations support that *Rhodospseudomonas* was the main electroactive PPB in the biofilm since the proteomic data reveals that this taxon encounters the most significant reorganization of its central carbon metabolism when growing under photoelectrochemical conditions. However, why did *Rhodospseudomonas* upregulate its catabolism? Table 3 shows the fold changes (FC) of the PC and PEPC enzymes, exhibiting a downregulation under photoelectrochemical conditions for *Wolinella* at the reactor's level. These data could suggest that *Wolinella* found a metabolic advantage in the increment of TCA metabolism of *Rhodospseudomonas* but also have to be interpreted considering the decreased abundance of this genera in the consortium. The FC values were thus re-calculated at the taxon's level for the *Wolinella* genus, and the only enzymes highlighted at this level (statically significant) were fumarate reductase proteins: fumarate reductase cytochrome b subunit (P17413),

fumarate reductase flavoprotein subunit (P17412), and fumarate reductase iron-sulfur subunit (P17596). The FC for these enzymes were 0.49 (ρ value 4.51E-02), 0.78 (ρ value 2.08E-02), and 0.63 (ρ value 1.61E-03), respectively. Fumarate reductase is the enzyme *Wolinella* needs to make possible fumarate respiration (fumarate + a reduced electron donor → succinate + oxidized electron donor), allowing anaerobic respiration. The reduced electron donor can be NADH, formate, or even H₂⁴¹. Fumarate is generated by the rTCA in chemotrophic dark conditions as the main pathway for malic acid catabolism (see Supporting Information, Supplementary Fig. S6). The decreased abundance of fumarate reductase of *Wolinella* at the taxon level indicates that this genus is reducing the activity of fumarate respiration, likely because of a commensalism ecological relation between PPB and *Wolinella*. In this sense, *Wolinella* could take advantage of the presence of PPB under photoelectrochemical conditions by taking succinate from the PPB metabolism (i.e., by direct interspecies transfer). The exact nature of this commensalism relationship will require further investigation.

Finally, the metaproteomic data (Fig. 7) and PHA analysis (Fig. 5) demonstrate that PHA accumulation is enhanced under photoelectrochemical conditions by the mixed biofilm of PPB using malic as a carbon source. The total percentage of PHA analyzed from the biofilm at different voltages exhibited an increase in PHA accumulation under electrochemical conditions, reaching a maximum content in the biomass at -0.4 V (23.8% d.w. of total PHA) (Fig. 5). In addition, the abundance of PHA synthesis-related enzymes from PPB genera at the reactor's level (Table 1) increased for all electrochemical experiments. Furthermore, some PHA enzymes are upregulated at the taxon level, especially for the *Rhodospseudomonas* genus (Fig. 7a, c). It is usually mentioned that an excess of carbon source or nutrient-limited conditions is necessary to enhance the accumulation of PHA^{16,48}. Still, the observed rise in PHA content was here obtained with fully balanced nutrient conditions, so the excess of electrons from the cathode is the only driver for this PHA accumulation.

The biosynthesis of PHA allows the dissipation of the excess NADPH, so this route depends on the substrate employed^{16,49,50}. For this reason, the

redox state of the carbon source is critical to optimizing PHA production by *R. palustris* TIE-1¹⁵. Touloupakis et al. used malate as a carbon source to study the accumulation of PHB. Still, they did not achieve it because of the lack of acetyl-coenzyme A produced by *Rhodospseudomonas sp.* in the presence of malate¹⁶. Also, Bayon-Vicente et al. studied the influence of different C sources on PHA accumulation, comparing succinate and valerate⁵¹. They showed that the abundance of PHA under succinate conditions was undetectable. Thereby, C sources such as malate and succinate do not enable the biosynthesis of PHA because of the lack of electrons and available acetyl-coenzyme A. Bayon-Vicente et al. also linked the production of PHA to a sudden increase of light intensity when *Rs. rubrum* was growing with acetate as sole carbon source. This PHA synthesis was also proposed to be linked to an excess of reducing equivalent¹⁷ as no nutrient limitation was present in their conditions, as in the current work.

A previous paper demonstrated that PHA accumulation is possible under photoelectroautotrophic conditions with a pure culture of *R. palustris* TIE-1; they only achieve 4.48 ± 0.11 mg PHB/L¹⁵. In contrast, this work found a significantly higher PHB accumulation under photoelectroheterotrophic conditions of 58.23 ± 2.81 and 17.59 ± 1.55 mg PHB/L at -0.4 and -0.8 V, respectively. However, the voltage that showed the best PHA accumulation in this work is lower than the voltage used by the cited work⁵²: -0.4 vs. -0.1 V (vs. Ag/AgCl), respectively, which means PHA accumulation is enhanced under lower voltages, as corroborated the up-regulation of PHA synthesis enzymes, at taxon's level, showed in Fig. 7. This data confirms that the enhancement of PHA synthesis is possible in heterotrophic conditions and with a mixed culture of PPB. As explained before, the excess of electrons supplied to the biofilm provoked a redox imbalance in PPB, generating excess reductive power inside the cell.

Implications for developing microbial photo-electrosynthesis devices

Bioelectrosynthesis relies on upgrading CO₂ into valuable commodities, but electrosynthetic bacteria usually leads to one compound-one metabolic pathway (e.g., cathodic electrofermentation or electromethanogenesis)⁵³. This work demonstrated that PPB grown in mixed-culture conditions are versatile enough to capture CO₂ by refixation in a heterotrophic system, allowing the conversion of oxidized substrates like malic acid into PHA, with no metabolite production. The implications for environmental biotechnology are vast. Biomass yield enhancement is quite interesting in applications like microbial protein production, where, as demonstrated here, biomass and protein yields are increased by more than 50% compared to non-BES processes (Fig. 4). Nevertheless, the most exciting outcome derived directly from this work is the possibility of converting oxidized compounds into PHA in a single-step process, with no energy mediators, thus avoiding the need for a pre-treatment process to convert organic feedstock rich in sugars and dicarboxylic acids into short-chain monocarboxylic acids (Fig. 5). These results also suggest using PPB-BES technology for applications related to fixing CO₂ (like biogas upgrading or photo-MES) and converting an organic waste source into bioplastics. We anticipate a rapid advance of this technology that can contribute to overcoming the global GHG reduction problem.

Methods

Preparation of synthetic medium, enrichment of PPB, and biofilm formation

Carbon and inorganic nitrogen sources were supplied as L-malic acid and ammonium chloride sources with a concentration of 2000 mg chemical oxygen demand (COD)/L and 300 mgN/L, respectively. The CO₂ obtained in the reactor is due to the oxidation of malic acid in the tricarboxylic acid cycle (TCA), allowing to focus on CO₂ fixation routes without any external source of this gas. The N source was ammonium to inhibit the hydrogen production¹², so we concentrate on internal electron dissipation mechanisms (mainly the Calvin–Benson–Bassham -CBB- cycle and the accumulation of polyhydroxyalkanoates (PHA)) instead of the external hydrogen evolution. Macro and micronutrients were prepared following the Ormerod

recipe⁵⁴. All chemical compounds came from Sigma-Aldrich (Merck KGaA, Darmstadt, Germany). The enrichment of the initial culture was carried out from a residual water sample. A 1 L suspended growth reactor with sludge liquor was inoculated, and subsequent incubation under near infra-red-light illumination and anaerobic conditions using synthetic wastewater as growth medium²⁷. Supporting Information (Supplementary Fig. S1) includes a picture of the resulting biofilm.

Photo-bioelectrochemical experiments

The photo-bioelectrochemical experiments were performed using a 0.5L glass H-type BES²⁷. The photo-bioelectrochemical experiments with PPB biofilm aim to determine the metabolic routes affected by the electrochemical conditions under different voltages tested, especially those pathways related to CO₂ fixation and PHA accumulation. Thereby, two consecutive photo-bioelectrochemical experiments, in batch mode, were conducted at room temperature (20°C) by progressively varying the voltage after cycles of 3 weeks (21 days for each experiment): -0.4 and -0.8 V, compared to the Ag/AgCl (3.5 M) reference electrode. The biofilm was adapted to the new voltage conditions during the first week. For the second week, sampling was performed daily to analyze pH, the absorbance of the liquid, CO₂ concentration at headspace, total inorganic carbon (TIC), soluble chemical oxygen demand (COD), and short-chain carboxylic acids (SCCA). Total COD, absorbance spectrum (450–950 nm), volatile suspended solids (VSS) from biofilm and liquid medium, and DNA samples from the biofilm were collected at the beginning and the end of the week. The samples for the metaproteomic analysis were taken during the last week of every cycle. CV tests (range of -1 to 1 V versus Ag/AgCl with a scan rate of 1 mV/s) were performed throughout the BES operation to determine the biocathode's electroactive behavior. A detailed summary of the experimental rationale and design can be accessed in Supporting Information (Supplementary Fig. S7).

Additional control experiments were also performed for one week: (i) a photobiological control (open circuit -OC-) with a PPB biofilm formed in a graphite bar to evaluate the contribution of the PPB metabolism in the absence of current intensity, (ii) a control without light (dark open circuit -DOC-) neither current, with a biofilm over the graphite bar to study the contribution of fermentative bacteria to organic matter degradation (iii) an electrochemical control (abiotic) at -0.8 V with a graphite bar without the PPB biofilm. The initial pH used for all biological experiments was 6.74 ± 0.09 to ensure an optimal medium for PPB growth.

In all BES experiments, the cathode and anode chambers were filled with the nitrogen source (NH₄Cl), the macro-, and the micronutrient solutions of the Ormerod medium⁵⁴. The carbon source was added to the cathode chamber to allow the microorganism to grow in this chamber only under continuous stirring. The medium and headspace of each chamber were flushed with argon to provide an anaerobic ambient. The cathode and anode liquid media were refreshed at the beginning of each experimental week, cleaning bacteria attached to the glass surface to enhance light penetration. Liquid samples were taken from the cathode and anode chambers and analyzed daily to monitor the experiment. Likewise, the current intensity of each experiment was monitored throughout the experiment. CVs were made on the second week of each experiment on days 0, 2, and 4 to measure the electroactivity of the biofilm.

Analytical methods

The BChl_a of PPB was detected by analyzing the VIS-NIR spectra (400–950 nm) using a UV-vis spectrophotometer (V-630, Jasco, Madrid, Spain). Total and soluble COD and volatile suspended solids (VSS) were determined according to standard methods⁵⁵. SCCAs were analyzed using an HPLC with the method described by Ventura et al.⁵⁶. The pH and EC were measured with a pH meter (GLP 22, Hach Lange Spain, Barcelona, Spain) and an electrical conductivity meter (912 Conductometer, Metrohm, Switzerland), respectively. Biomass concentration was determined using a standard curve of PPB optical density and volatile suspended solids (gVSS/L)

concentration. The total biomass, in terms of mg COD/L, was calculated as the difference between the total COD and soluble COD using Eq. [1]. The fraction of biomass from biofilm in mg COD/L was calculated using the Eq. [2], assuming a COD/VSS ratio for PPB of 1.61¹ and COD/VSS ratio for non-PPB of 1.42², and percentages of PPB and Non-PPB microorganisms in the biofilm estimated according to genus data from microbial community analyses.

$$\text{COD}_{\text{total}} - \text{COD}_{\text{soluble}} = \text{COD}_{\text{particulate}} \quad (1)$$

$$(\text{VSS}_{\text{PPB}} \cdot \% \text{PPB}) \cdot 1.61 + (\text{VSS}_{\text{non-PPB}} \cdot \% \text{Non-PPB}) \cdot 1.42 = \text{COD}_{\text{biofilm}} \quad (2)$$

The optical density of PPB biomass was measured at 665 and 850 nm by UV-VIS spectrophotometer (V-630, Jasco, Madrid, Spain). TIC was analyzed by a combustion/non-dispersive infrared gas analyzer (Shimadzu TOC 5000A). The biomass attached to the cathode's surface was quantified experimentally by taking samples directly from the cathode by scraping the cathode with a blade and measuring the biomass recovery from the blade surface in a separate vessel of 5 mL volume. In order to homogenize the biomass recovery in the vessel, the vessel was submitted to ultrasounds in an ultrasound bath, and the biomass was further dispersed by using a vial shaker. The concentration of biomass attached on the surface was quantified using the Eq. [3]:

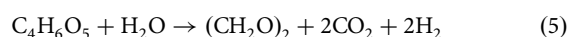
$$\frac{\text{VSS}_T \frac{V_i}{1000} \frac{S_T}{S_i}}{V_T} = \text{VSS}_T \quad (3)$$

Where VSS_i are the measured VSS (mg/L) in the 5 mL vessel, V_i is the vessel volume (5 mL), S_i is the scratched surface (in cm²) and S_T is the total surface of the electrode (in cm²), V_T is the volume of the reactor (0.5 L), and VSS_T is the concentration of attached biomass in relation of the reactor's volume (mgVSS/L). The PHA content was calculated as PHA production yield (expressed as wt.% on a dry basis). The extraction and analysis of PHA content are reported by Allegue et al.⁵⁷. All samples used for analyzing soluble components were filtered with 0.45 μm nylon filters (Chrodisc filter/syringe, CHMLab Barcelona, Spain). Total COD, *BChla*, optical density of PPB biomass, and VSS concentration were determined using non-filtered samples.

The total amount of CO₂ present in the cathode chamber was calculated by adding up the total inorganic carbon (TIC) in the aqueous medium and the amount of CO₂ analyzed in the head space, expressed as mg of inorganic carbon (mg IC). The calculation to obtain the total IC in the reactor is described in Eq. [4]. Besides, the theoretical amount of CO₂ produced from malic acid, calculated following the stoichiometry, we obtained the percentage of carbon dioxide fixed under bioelectrochemical conditions:

$$\text{CO}_2 (\text{mg IC}) = \frac{P \cdot V_{\text{HS}}}{R \cdot T} \cdot \frac{\text{CO}_2 \%}{100} \cdot \text{Mm} \cdot 0.27 \cdot 1000 \quad (4)$$

where *P* is the total pressure inside the cathode chamber, V_{HS} is the head-space volume in the cathode chamber, *R* is the ideal gases constant (0.082 atm L mol⁻¹ K⁻¹), *T* is the temperature of the laboratory (20 °C was used as an average temperature), CO₂% is the percentage of carbon dioxide detected by GC in the head space every day, Mm is the molecular mass of CO₂, 0.27 is the relation mg IC/mg CO₂, and 1000 is used to unit conversion. The reaction of malic consumption by the *Rhodospirillum rubrum* is:



The theoretical amount of CO₂ produced by malic degradation was calculated using the stoichiometry of this reaction. The mass of malate used was the experimental data determined at the beginning of each experiment.

The CO₂ calculated from this reaction is considered the theoretical CO₂ obtained by PPB from malic acid, via TCA.

The percentage of CO₂ consumed was calculated using the experimental data of CO₂ (as mg IC) from the day when the COD was almost completely consumed, that is the day when the amount of CO₂ (produced due to malic degradation by microorganism) is the maximum.

The composition of the microbial community has been analyzed through Illumina MiSeq. The DNA from the biomass samples is previously extracted with a HigherPurity™ Bacterial Genomic DNA Isolation Kit by Canvax Biotech (Córdoba, Spain). After that, the extracted DNA samples were sent to FISABIO Sequencing and Bioinformatics (Valencia, Spain) for 16s rRNA gene amplicon sequencing following the 16S rDNA gene Metagenomic Sequencing Library Preparation Illumina protocol (Cod. 15044223 Rev. A). The primers are selected from ref. 58. The full-length primer sequences, using standard IUPAC nucleotide nomenclature, are: 16S V3-V4 Forward: TCGTCGGCAGCGTCAGATGTGTATAAGAGACAG CCTACGGGNGGCWGCAG and 16S V3-V4 Reverse: GCTCTGTGG GCTCGGAGATGTGTATAAGAGACAGGACTACHVGGGTATCTAA TCC. Microbial genomic DNA (5 ng/μl in 10 mM Tris pH 8.5) was used to initiate the protocol. After 16S rDNA gene amplification, the multiplexing step was performed using Nextera XT Index Kit (FC-131-1096). After size verification, the libraries were sequenced using a 2x300pb paired-end run (MiSeq Reagent kit v3 (MS-102-3001)) on a MiSeq Sequencer. Denoising, paired-ends joining, and chimera depletion were performed starting from paired ends data using the DADA2 pipeline⁵⁹. The database used for the taxonomic assignation was the Silva138⁶⁰. Data handling regarding microbiologic analysis was done using an RStatistics environment.

A quantitative metaproteomic analysis was performed on proteins extracted from mixed biofilm for each photo-bioelectrochemical experiment and open circuit control. Proteins were extracted in a guanidine HCl 6 M, K₂HPO₄ 50 mM buffer by sonication (3 × 10 s, amplitude 20%)⁶¹. Tryptic peptides were analyzed in Data Dependent Acquisition mode⁶², and the TripleTof 6600 from Sciex was used for data acquisition. Data were searched using Protein Pilot 4.2 against a Uniprot extracted proteome containing the main genera detected through the microbial community analysis. The sequence database included the following genera: *Rhodobacter*, *Rhosopseudomonas*, *Rubrivivax*, *Wolinella*, *Shewanella*, *Desulfovivrio*, and *Enterococcus*. Methionine oxidation and cysteine carbamidomethylation were set up as variable and fixed modifications, respectively. Proteins were quantified using skyline in “precursor” mode, only with unmodified peptides, not considering peptides originating from trypsin missed cleavages. To allow confident protein assignment to the considered taxa, only unique peptides were used and all shared peptides (belonging to multiple taxa) were removed for the quantification. The areas under the curve were exported in Excel for student t-test evaluation of the significance. The selection of relevant enzymes from metaproteomic data was made by searching manually the enzymes involved in metabolic routes of interest: TCA, CBB, PHA synthesis, anaerobic CO₂ fixation, and extracellular electron uptake mechanism⁶³⁻⁶⁶. Protein abundances were processed to gain modification data at reactor and taxon levels. In the first case, protein abundance normalization was performed by equalization of the median using the entire dataset across the replicates. This usual procedure allows for mitigating potential bias in protein loading across replicates and enables the calculation of abundance modification at the reactor level but does not consider the modification in relative abundance of the protein. In other words, if a species' abundance is twice as abundant in a sample as in the control, even without any gene expression change, all the proteins from this species will appear with a fold change of 2. As the microbial consortium composition also varied during the experiment and as our goal was to analyze the regulation of protein abundance at the taxon level, we used a second normalization strategy to produce quantitative data at the taxon level. To obtain this taxon's level information, we considered only the four most abundant species, and normalizations were performed by equalization of the median across replicates but separately for each

selected species. This procedure allows for the mitigation of changes in the relative abundance of a species in the studied consortium.

The selection of relevant enzymes from metaproteomic data was made by searching manually the enzymes involved in metabolic routes of interest: TCA, CBB, PHA synthesis, anaerobic CO₂ fixation, and extracellular electron uptake mechanism^{63–66}. The fold change parameter was calculated as the relative ratio of each protein between two conditions (photo-bioelectrochemical experiment vs. open circuit control)⁶⁷. Every sample was made by triplicate, and the average value of the area was used to estimate FC as it represented in Eq. [4]

$$FC = \text{Area}_{\text{PBE}} / \text{Area}_{\text{OC}} \quad (6)$$

where Area_{PBE} is the area of the protein from the Photo-BioElectrochemical experiment and Area_{OC} is area of the protein from the Open Circuit control. The data used to study the taxon level changes between experiments was normalized to calculate the FC. The areas of proteins were individually normalized based on a summed area of all peptides for each sample. Only fold change higher than 1.5 or lower than 0.66 and having a *p*-value lower than 0.05 for reactor's level estimations, and lower than 0.1 for taxons' level estimations, were further considered¹⁷. To make the volcano plots' figures of the proteins quantified, the log₁₀(*p*-value) was calculated and plotted against the log₂(FC)¹⁷.

Statistics and reproducibility

The data provided in the bar graphs (Figs. 3–5) correspond to the average value of 3 measurements taken during 5 successive days, after a steady response was reached. To discern the effect of the polarization, the first week of each condition was used as an acclimation period. Statistical significance was analyzed by calculating the confidence intervals (at 95%) (CI95) for all the experimental data and the estimated parameters. Variation intervals in all tables and error bars in all figures represent CI95.

Reporting summary

Further information on research design is available in the Nature Portfolio Reporting Summary linked to this article.

Data availability

The data supporting the findings of this study are available within the article and its Supporting Information. Supplementary Data includes all the data from the Figures, including main statistical parameters, and the data from the metaproteomic calculations and the taxonomical analysis. Full metaproteomic data has been deposited on PRIDE, with the dataset identifier PXD051223. In addition, complete experimental, metaproteomic, and taxonomy data are available from the corresponding authors upon reasonable request.

Received: 17 January 2023; Accepted: 31 October 2024;

Published online: 18 November 2024

References

- European Commission. *Communication from the Commission to the European Parliament, the Council, the European Economic and Social Committee and the Committee of the Regions: A Policy Framework for Climate and Energy in the Period from 2020 to 2030* (2014).
- UNFCCC, U. N. F. C. on C. C. *Glasgow Climate Pact*. 1–11 (2021).
- Madejski, P., Chmiel, K., Subramanian, N. & Kuś, T. Methods and techniques for CO₂ capture: review of potential solutions and applications in modern energy technologies. *Energies (Basel)* **15**, 887 (2022).
- Almomani, F., Abdelbar, A. & Ghanimeh, S. A Review Of The Recent Advancement Of Bioconversion Of Carbon Dioxide To Added Value Products: A State Of The Art. *Sustainability* **15**, 10438 (2023).
- Nisar, A. et al. Bio-conversion of CO₂ into biofuels and other value-added chemicals via metabolic engineering. *Microbiol Res.* **251**, 126813 (2021).
- George, D. M., Vincent, A. S. & Mackey, H. R. An overview of anoxygenic phototrophic bacteria and their applications in environmental biotechnology for sustainable Resource recovery. *Biotechnol. Rep.* **28**, e00563 (2020).
- Capson-Tojo, G. et al. Purple phototrophic bacteria for resource recovery: challenges and opportunities. *Biotechnol. Adv.* **43**, 107567 (2020).
- Batstone, D. J., Hülsen, T., Mehta, C. M. & Keller, J. Platforms for energy and nutrient recovery from domestic wastewater: A review. *Chemosphere* **140**, 2–11 (2015).
- Puyol, D. et al. *Purple Phototrophic Bacteria As A Platform To Create The Next Generation Of Wastewater Treatment Plants: Energy And Resource Recovery* (eds. Olivares, J. A., Puyol, D., Melero, J. A. & Dufour, J. B. T.-W. T. R.) 255–280 (Elsevier, 2020).
- McKinlay, J. B. & Harwood, C. S. Carbon dioxide fixation as a central redox cofactor recycling mechanism in bacteria. *Proc. Natl Acad. Sci. USA* **107**, 11669–11675 (2010).
- Alloul, A. et al. Dehazing redox homeostasis to foster purple bacteria biotechnology. *Trends Biotechnol.* **41**, 106–119 (2022).
- Vasiliadou, I. A. et al. Biological and bioelectrochemical systems for hydrogen production and carbon fixation using purple phototrophic bacteria. *Front. Energy Res.* **6**, 12 (2018).
- Vasiliadou, I. A., Melero, J. A., Molina, R., Puyol, D. & Martinez, F. Optimization of H₂ production through minimization of CO₂ emissions by mixed cultures of purple phototrophic bacteria in aqueous samples. *Water (Basel)* **12**, 2015 (2020).
- Fradinho, J. et al. Up-scale challenges on biopolymer production from waste streams by Purple Phototrophic Bacteria mixed cultures: a critical review. *Bioresour. Technol.* **327**, 124820 (2021).
- Ranaivoarisoa, T. O., Singh, R., Rengasamy, K., Guzman, M. S. & Bose, A. Towards sustainable bioplastic production using the photoautotrophic bacterium *Rhodospseudomonas palustris* TIE-1. *J. Ind. Microbiol Biotechnol.* **46**, 1401–1417 (2019).
- Touloupakis, E., Poloniataki, E. G., Ghanotakis, D. F. & Carozzi, P. Production of Biohydrogen and /or Poly- β -hydroxybutyrate by *Rhodospseudomonas* sp. using various carbon sources as substrate. *Appl. Biochem. Biotechnol.* <https://doi.org/10.1007/s12010-020-03428-1> (2021).
- Bayon-Vicente, G., Wattiez, R. & Leroy, B. Global proteomic analysis reveals high light intensity adaptation strategies and polyhydroxyalkanoate production in *Rhodospirillum rubrum* cultivated with acetate as carbon source. *Front. Microbiol.* **11**, 1–17 (2020).
- Grattieri, M. Purple bacteria photo-bioelectrochemistry: enthralling challenges and opportunities. *Photochem. Photobiol. Sci.* **19**, 424–435 (2020).
- Bian, B., Bajracharya, S., Xu, J., Pant, D. & Saikaly, P. E. Microbial electrosynthesis from CO₂: challenges, opportunities and perspectives in the context of circular bioeconomy. *Bioresour. Technol.* **302**, 122863 (2020).
- Dessi, P. et al. Microbial electrosynthesis: towards sustainable biorefineries for production of green chemicals from CO₂ emissions. *Biotechnol. Adv.* **46**, 107675 (2021).
- Bose, A., Gardel, E. J., Vidoudez, C., Parra, E. A. & Girguis, P. R. Electron uptake by iron-oxidizing phototrophic bacteria. *Nat. Commun.* **5**, 3391 (2014).
- Rengasamy, K., Ranaivoarisoa, T., Singh, R. & Bose, A. An insoluble iron complex coated cathode enhances direct electron uptake by *Rhodospseudomonas palustris* TIE-1. *Bioelectrochemistry* **122**, 164–173 (2018).
- Guzman, M. S. et al. Phototrophic extracellular electron uptake is linked to carbon dioxide fixation in the bacterium *Rhodospseudomonas palustris*. *Nat. Commun.* **10**, 1–13 (2019).

24. Li, S. et al. Photoautotrophic hydrogen production of *Rhodobacter sphaeroides* in a microbial electrosynthesis cell. *Bioresour. Technol.* **320**, 124333 (2021).
25. Liao, X., Pan, Q., Tian, X., Wu, X. & Zhao, F. Proteomic analysis of the electron uptake pathway of *Rhodospseudomonas palustris* CGA009 under different cathodic potentials. *Process Biochem.* **115**, 42–48 (2022).
26. Nguyenhuynh, T., Yoon, L. W., Chow, Y. H. & Chua, A. S. M. An insight into enrichment strategies for mixed culture in polyhydroxyalkanoate production: feedstocks, operating conditions and inherent challenges. *Chem. Eng. J.* **420**, 130488 (2021).
27. Díaz-Rullo Edreira, S. et al. Assessment of voltage influence in carbon dioxide fixation process by a photo-bioelectrochemical system under photoheterotrophy. *Microorganisms* **9**, 1–8 (2021).
28. Kitching, M., Butler, R. & Marsili, E. Microbial bioelectrosynthesis of hydrogen: current challenges and scale-up. *Enzym. Micro. Technol.* **96**, 1–13 (2017).
29. Henderson, R. K., Baker, A., Parsons, S. A. & Jefferson, B. Characterisation of algogenic organic matter extracted from cyanobacteria, green algae and diatoms. *Water Res.* **42**, 3435–3445 (2008).
30. Zhang, X. et al. Rapid and quantitative assessment of redox conduction across electroactive biofilms by using double potential step chronoamperometry. *ChemElectroChem* **4**, 1026–1036 (2017).
31. Choi, O. & Sang, B. I. Extracellular electron transfer from cathode to microbes: application for biofuel production. *Biotechnol. Biofuels* **9**, 1–14 (2016).
32. Shi, L. et al. Molecular underpinnings of Fe(III) oxide reduction by *Shewanella oneidensis* MR-1. *Front. Microbiol.* **3**, 50 (2012).
33. Pitts, K. E. et al. Characterization of the *Shewanella oneidensis*. *J. Biol. Chem.* **278**, 27758–27765 (2003).
34. Gorby, Y. et al. Redox-reactive membrane vesicles produced by *Shewanella*. *Geobiology* **6**, 232–241 (2008).
35. Hartshorne, R. S. et al. Characterization of *Shewanella oneidensis* MtrC: a cell-surface decaheme cytochrome involved in respiratory electron transport to extracellular electron acceptors. *J. Biol. Inorg. Chem.* **12**, 1083–1094 (2007).
36. Conners, E. M., Rengasamy, K. & Bose, A. Electroactive biofilms: how microbial electron transfer enables bioelectrochemical applications. *J. Ind. Microbiol. Biotechnol.* **49**, kuac012 (2022).
37. Jiao, Y. & Newman, D. K. The *pio* operon is essential for phototrophic Fe(II) oxidation in *Rhodospseudomonas palustris* TIE-1. *J. Bacteriol.* **189**, 1765–1773 (2007).
38. Dinesh, G. et al. Photoferrotophys produce a *PioAB* electron conduit for extracellular electron uptake. *mBio* **10**, e02668–19 (2019).
39. Guardia, A. E., Beligni, M. V., Cortés, N. & Busalmen, J. P. Electrochemistry of *R. palustris* Azul during phototrophic growth. *Electrochim Acta* **355**, 136757 (2020).
40. Grattieri, M., Rhodes, Z., Hickey, D. P., Beaver, K. & Minteer, S. D. Understanding Biophotocurrent Generation in Photosynthetic Purple Bacteria. *ACS Catal.* **9**, 867–873 (2019).
41. Gest, H. et al. Studies on the metabolism of photosynthetic bacteria. *J. Biol. Chem.* **182**, 153–170 (1950).
42. Berman, H. M. et al. The Protein Data Bank. *Nucleic Acids Res* **28**, 235–242 (2000).
43. Madigan, M. T. *Brock, Brock Biology of Microorganisms* (Pearson Educación. Upper Saddle River, 2009).
44. Tang, K. H., Tang, Y. J. & Blankenship, R. E. Carbon metabolic pathways in phototrophic bacteria and their broader evolutionary implications. *Front Microbiol* **2**, 1–23 (2011).
45. Yurkov, V. V. & Beatty, J. T. Aerobic anoxygenic phototrophic bacteria. *Microbiol. Mol. Biol. Rev.* **62**, 695–724 (1998).
46. Tang, K.-H., Feng, X., Tang, Y. J. & Blankenship, R. E. Carbohydrate metabolism and carbon fixation in *Roseobacter denitrificans* OCh114. *PLoS ONE* **4**, 7233 (2009).
47. Fürch, T. et al. Metabolic fluxes in the central carbon metabolism of *Dinoroseobacter shibae* and *Phaeobacter gallaeciensis*, two members of the marine *Roseobacter* clade. *BMC Microbiol.* **9**, 209 (2009).
48. Higuchi-Takeuchi, M. & Numata, K. Marine purple photosynthetic bacteria as sustainable microbial production hosts. *Front. Bioeng. Biotechnol.* **7**, 258 (2019).
49. Chen, Y.-T., Wu, S. C. & Lee, C. Relationship between cell growth, hydrogen production and poly- β -hydroxybutyrate (PHB) accumulation by *Rhodospseudomonas palustris* WP3-5. *Int. J. Hydrog. Energy* **37**, 13887–13894 (2012).
50. Hustede, E., Steinbüchel, A. & Schlegel, H. G. Relationship between the photoproduction of hydrogen and the accumulation of PHB in non-sulphur purple bacteria. *Appl. Microbiol. Biotechnol.* **39**, 87–93 (1993).
51. Bayon-Vicente, G., Zarbo, S., Deutschbauer, A., Wattiez, R. & Leroy, B. Photoheterotrophic assimilation of valerate and associated polyhydroxyalkanoate production by *Rhodospirillum rubrum*. *Appl. Environ. Microbiol.* **86**, e00901–e00920 (2020).
52. Rengasamy, K., Ranaivoarisoa, T. O., Singh, R. & Bose, A. Improving microbial electrosynthesis of polyhydroxybutyrate (PHB) from CO₂ by *Rhodospseudomonas palustris* TIE-1 using an immobilized iron complex modified cathode. *Bioelectrochemistry* **122**, 164–173 (2018).
53. Wood, J. C. et al. Strategies to improve viability of a circular carbon bioeconomy-A techno-economic review of microbial electrosynthesis and gas fermentation. *Water Res.* **201**, 117306 (2021).
54. Ormerod, J. G., Ormerod, K. S. & Gest, H. Light-dependent utilization of organic compounds photoproduction of molecular hydrogen by photosynthetic bacteria; relationships with nitrogen metabolism. *Arch. Biochem. Biophys.* **94**, 449–463 (1961).
55. American Public Health Association (APHA), American Water Works Association (AWWA) & Water Environment Federation (WEF). *Standard Methods for the Examination of Water and Wastewater* (Washington, D.C, 2005).
56. Ventura, M., Puyol, D. & Melero, J. A. The synergy of catalysis and biotechnology as a tool to modulate the composition of biopolymers (polyhydroxyalkanoates) with lignocellulosic wastes. *Catal. Today* **9**, 1996 (2021).
57. Allegue, L. D., Ventura, M., Melero, J. A. & Puyol, D. Integrated sustainable process for polyhydroxyalkanoates production from lignocellulosic waste by purple phototrophic bacteria. *GCB Bioenergy* **13**, 862–875 (2021).
58. Klindworth, A. et al. Evaluation of general 16S ribosomal RNA gene PCR primers for classical and next-generation sequencing-based diversity studies. *Nucleic Acids Res.* **41**, e1–e1 (2013).
59. Callahan, B. J. et al. DADA2: high-resolution sample inference from Illumina amplicon data. *Nat. Methods* **13**, 581–583 (2016).
60. Quast, C. et al. The SILVA ribosomal RNA gene database project: Improved data processing and web-based tools. *Nucleic Acids Res.* **41**, D590 (2013).
61. Cabecas Segura, P. et al. Effects of mixing volatile fatty acids as carbon sources on *rhodospirillum rubrum* carbon metabolism and redox balance mechanisms. *Microorganisms* **9**, 1996 (2021).
62. Contreras, A., Leroy, B., Mariage, P.-A. & Wattiez, R. Proteomic analysis reveals novel insights into tanshinones biosynthesis in *Salvia miltiorrhiza* hairy roots. *Sci. Rep.* **9**, 5768 (2019).
63. Caspi, R. et al. The MetaCyc database of metabolic pathways and enzymes and the BioCyc collection of Pathway/Genome Databases. *Nucleic Acids Res.* **42**, D459–D471 (2014).
64. UniProt Consortium, The UniProt: the universal protein knowledgebase in 2021. *Nucleic Acids Res.* **49**, D480–D489 (2021).
65. Cabecas Segura, P. et al. Study of the production of poly(hydroxybutyrate-co-hydroxyhexanoate) and poly(hydroxybutyrate-co-hydroxyvalerate-co-hydroxyhexanoate) in *Rhodospirillum rubrum*. *Appl. Environ. Microbiol.* <https://doi.org/10.1128/AEM.01586-21> (2022).

66. Fradinho, J. C., Oehmen, A. & Reis, M. A. M. Photosynthetic mixed culture polyhydroxyalkanoate (PHA) production from individual and mixed volatile fatty acids (VFAs): substrate preferences and co-substrate uptake. *J. Biotechnol.* **185**, 19–27 (2014).
67. Aguilan, J. T., Kulej, K. & Sidoli, S. Guide for protein fold change and P-value calculation for non-experts in proteomics. *Mol. Omics* **16**, 573–582 (2020).

Acknowledgements

This work has been partially funded by the Spanish Ministry of Economy by the FOTOBIOELECTRO project (CTM2017-91186-EXP) and the Community of Madrid through projects REMTAVARES-CM (S2018/EMT-4341) and BIOTRES-CM (S2018/EMT-4344). D.P. also acknowledges the Spanish Ministry of Economy for the concession of a Ramon y Cajal grant. Funding received from the Community of Madrid and the University Rey Juan Carlos through the R&D Young Researchers Fund 2019 (project SUN-BIOELECTROMAT) is also acknowledged. Work of B.L. and R.W. was supported by CDR funding “Redox homeostasis in purple bacteria” (CDR FRS FNRS). The Bio-profiling platform used for proteomic analysis was supported by the European Regional Development Fund and the Walloon Region, Belgium.

Author contributions

S.D.-R.E. helped design the experiments, carried out the bioelectrochemical experiments, calculated electrochemical parameters, created the metabolic pictures, carried out the analytical measurements, analyzed the data, and wrote the manuscript. I.A.V. wrote the introduction section and revised the manuscript. A.P. helped calculate electrochemical parameters and revised the manuscript. J.J.E. supervised the project and helped writing the manuscript. R.W. and B.L. performed metaproteomic analyses, analyzed the data and revised the manuscript. F.M. supervised the project, analyzed the data, and helped write the manuscript. D.P. conceived the idea, supervised the project, design the experiments, analyzed the data, and wrote the manuscript. All the authors commented on the manuscript and have given approval for the final version of the manuscript.

Competing interests

The authors declare no competing interests.

Additional information

Supplementary information The online version contains supplementary material available at <https://doi.org/10.1038/s42003-024-07188-0>.

Correspondence and requests for materials should be addressed to Daniel Puyol.

Peer review information *Communications Biology* thanks Matteo Grattieri and the other, anonymous, reviewer(s) for their contribution to the peer review of this work. Primary Handling Editors: Thulani Makhalanyane and David Favero. A peer review file is available.

Reprints and permissions information is available at <http://www.nature.com/reprints>

Publisher's note Springer Nature remains neutral with regard to jurisdictional claims in published maps and institutional affiliations.

Open Access This article is licensed under a Creative Commons Attribution-NonCommercial-NoDerivatives 4.0 International License, which permits any non-commercial use, sharing, distribution and reproduction in any medium or format, as long as you give appropriate credit to the original author(s) and the source, provide a link to the Creative Commons licence, and indicate if you modified the licensed material. You do not have permission under this licence to share adapted material derived from this article or parts of it. The images or other third party material in this article are included in the article's Creative Commons licence, unless indicated otherwise in a credit line to the material. If material is not included in the article's Creative Commons licence and your intended use is not permitted by statutory regulation or exceeds the permitted use, you will need to obtain permission directly from the copyright holder. To view a copy of this licence, visit <http://creativecommons.org/licenses/by-nc-nd/4.0/>.

© The Author(s) 2024